



Intersectin deficiency impairs cortico-striatal neurotransmission and causes obsessive–compulsive behaviors in mice

Dennis Vollweiter^{a,b}, Jasmeet Kaur Shergill^b, Alexandra Hilse^b, Gaga Kochlamazashvili^a, Stefan Paul Koch^{c,d,e}, Susanne Mueller^{c,d,e}, Philipp Boehm-Sturm^{c,d,e}, Volker Haucke^{a,f,g,1}, and Tanja Maritzen^{a,b,1}

Edited by Reinhard Jahn, Max Planck Institute for Multidisciplinary Science, Goettingen, Germany; received March 15, 2023; accepted July 24, 2023

The generation of appropriate behavioral responses involves dedicated neuronal circuits. The cortico-striatal-thalamo-cortical loop is especially important for the expression of motor routines and habits. Defects in this circuitry are closely linked to obsessive stereotypic behaviors, hallmarks of neuropsychiatric diseases including autism spectrum disorders (ASDs) and obsessive–compulsive disorders (OCDs). However, our knowledge of the essential synaptic machinery required to maintain balanced neurotransmission and plasticity within the cortico-striatal circuitry remains fragmentary. Mutations in the large synaptic scaffold protein intersectin1 (ITSN1) have been identified in patients presenting with ASD symptoms including stereotypic behaviors, although a causal relationship between stereotypic behavior and intersectin function has not been established. We report here that deletion of the two closely related proteins ITSN1 and ITSN2 leads to severe ASD/OCD-like behavioral alterations and defective cortico-striatal neurotransmission in knockout (KO) mice. Cortico-striatal function was compromised at multiple levels in ITSN1/2-depleted animals. Morphological analyses showed that the striatum of intersectin KO mice is decreased in size. Striatal neurons exhibit reduced complexity and an underdeveloped dendritic spine architecture. These morphological abnormalities correlate with defects in cortico-striatal neurotransmission and plasticity as well as reduced N-methyl-D-aspartate (NMDA) receptor currents as a consequence of postsynaptic NMDA receptor depletion. Our findings unravel a physiological role of intersectin in cortico-striatal neurotransmission to counteract ASD/OCD. Moreover, we delineate a molecular pathomechanism for the neuropsychiatric symptoms of patients carrying intersectin mutations that correlates with the observation that NMDA receptor dysfunction is a recurrent feature in the development of ASD/OCD-like symptoms.

autism spectrum disorder | obsessive–compulsive disorder | stereotypy | knockout | NMDA receptors

Adaptive behavioral responses enable organismal survival in response to varying environmental conditions. The compulsion to carry out stereotypic motor routines severely interferes with the ability of affected individuals to cope with the challenges imposed by daily life. The compulsive execution of out-of-place behaviors is a hallmark of autism spectrum disorders (ASDs) and obsessive–compulsive disorders (OCDs), including Tourette's syndrome and trichotillomania, and affects ~2% of the world population (1, 2). Repetitive and stereotyped behaviors are in fact an early manifestation of ASDs being observable in 3 to 4-y-old children (3).

The generation of adequate behavioral responses takes place within complex neuronal circuits that rely on fine-tuned neurotransmission at the synapses involved. Mouse models and optogenetics approaches have revealed that the selection of motor programs and formation of habits is encoded within a cortico-striatal-thalamo-cortical neural loop. Complex motor programs are believed to be assembled within this circuitry by selecting short motor sequences and linking them together (4). Consequently, disturbances in neurotransmission along this pathway are envisioned to drive repetitive stereotyped behavioral patterns (4). In line with this, alterations in cortico-striatal transmission have been linked to repetitive behaviors in mouse models and patients (5, 6). In spite of this progress, our knowledge of the molecular machinery required to maintain and fine-tune efficient neurotransmission at cortico-striatal synapses and, thus, to safeguard against repetitive behaviors remains fragmentary. Recent studies have identified *de novo* variants in the gene encoding intersectin1 (ITSN1) in patients exhibiting ASD symptoms including stereotypes. While these data suggest a role for ITSN1 in the etiology of autosomal dominant neurodevelopmental disorders and repetitive behaviors (7), evidence for a causal role of ITSN1 dysfunction in neuropsychiatric disease is lacking.

We fill this important gap by demonstrating that deletion of both intersectin genes (i.e., ITSN1 and ITSN2) in mice leads to striking ASD/OCD-like behavioral alterations.

Significance

The compulsion to carry out stereotypic motor routines is a hallmark of neuropsychiatric diseases like autism spectrum and obsessive–compulsive disorders and interferes with the ability to cope with everyday life. The generation of appropriate motor behaviors involves circuitry connecting cortical and striatal brain areas. However, the synaptic machinery necessary to maintain balanced cortico-striatal neurotransmission is still elusive. Recently, mutations in intersectin1 (ITSN1) have been identified in patients with neurological symptoms including stereotypic behaviors. However, a causal relationship between intersectin and these symptoms has not been established. We show that deletion of ITSN1/2 in mice leads to stereotypic behavior, morphological abnormalities, and defective cortico-striatal neurotransmission linked to reduced N-methyl-D-aspartate (NMDA) receptor currents, delineating a pathomechanism for the symptoms of patients carrying intersectin mutations.

The authors declare no competing interest.

This article is a PNAS Direct Submission.

Copyright © 2023 the Author(s). Published by PNAS. This article is distributed under Creative Commons Attribution-NonCommercial-NoDerivatives License 4.0 (CC BY-NC-ND).

¹To whom correspondence may be addressed. Email: haucke@fmp-berlin.de or maritzen@rptu.de.

This article contains supporting information online at <https://www.pnas.org/lookup/suppl/doi:10.1073/pnas.2304323120/-DCSupplemental>.

Published August 21, 2023.

Intersectin double knockout (dKO) mice display obsessive and stereotypic jackhammer-like jumping in the corners of the cage consistent with the observation of stereotypic behaviors in patients carrying loss-of-function mutations in the *ITSN1* gene (7). Morphological and electrophysiological analyses revealed multiple defects in the cortico-striatal circuitry of *ITSN* dKO mice. Our results unravel a crucial role for intersectins in maintaining efficient cortico-striatal neurotransmission and appropriate motor behavior, thereby strengthening the link between human *ITSN1* mutations and ASD/OCD-like neuropsychiatric disorders.

Results

Loss of *ITSN1/2* Leads to Hyperactivity and Obsessive Stereotypic Behavior. To study the putative link between intersectin function and ASD/OCD-like disorders in humans, we generated dKO mice lacking the related scaffold proteins *ITSN1* and *ITSN2*. We observed that a fraction of dKO mice died pre- or postnatally (8). The remaining animals survived to adulthood and appeared healthy but exhibited reduced weight gain and were smaller. dKO mice were on average ~18% lighter compared to controls (8). As adult dKO mice exhibited profound changes in home cage behaviors, we subjected them to in-depth behavioral analyses starting with a 10 min observation of individual mice in their home cage environment. *ITSN2* KO (2KO) mice, which did not display alterations compared to wildtype littermates at any level of analysis (i.e., body weight, size, behavior, and anatomy) served as controls. Strikingly, a major fraction of dKO mice displayed an obsessive and stereotypic motor routine characterized by repeated jumping in the corner of the homecage (Movie S1). Jumping bouts of dKO mice lasted for seconds to minutes with up to 600 jumps occurring within the 10 min observation period, while control mice did not jump at all (Fig. 1A). At times dKO mice also stood upright in the corners of their cage and exhibited stereotypic running-like behavior at the cage wall (Fig. 1B) or showed abrupt changes of movement direction (Fig. 1C).

The number of wall rearings (Fig. 1D) and the number of grooming sessions (Fig. 1E) did not differ between dKOs and controls. These data suggest that dKO mice obsessively repeat specific sets of motor routines, akin to the presence of distinct forms of repetitive behaviors in ASD patients. This notion was further confirmed by the marble burying test in which dKO mice unlike controls failed to bury any marbles (Fig. 1F). Similar observations have been made in other mouse models of ASD (9, 10). dKO mice also spent less time dealing with paper towels supplied in their cages (Fig. 1G) and failed to build proper nests (Fig. 1H), another feature frequently observed in ASD-like mouse models (9, 11–13). To quantitatively assess these behavioral abnormalities, we tracked the movement of control and dKO mice in xyz by monitoring infrared light beam breaks for 24 h in a home cage environment. This analysis confirmed that dKO mice spend significantly more time in the periphery of their cages, as evidenced by movement plots (Fig. 1I). Repetitive z-beam breaks as indicators of stereotypic jumping revealed that dKO mice performed on average >50,000 jumps within 24 h (Fig. 1J). In addition, dKO mice were hyperactive as evidenced by an increased distance traveled (Fig. 1K) and elevated average locomotion speed (Fig. 1L). The obsessive perseverance in a specific stereotypic behavior observed in the dKO mice is highly reminiscent of neuropsychiatric diseases including ASD and OCD (6). Importantly, it was also found in a subset of patients with truncating or missense mutations in *ITSN1* (7).

To further investigate potential parallels to mouse models of neuropsychiatric diseases, we used an elevated plus maze assay to

probe anxiety-like behavior, which is often altered in such models. Akin to some mouse models of ASD (10), fragile X syndrome (14), and Down syndrome (15) [but in contrast to others (13, 16, 17)], *ITSN* dKO mice exhibited reduced anxiety-like behavior as reflected by spending more time on the open arms of the elevated plus maze (SI Appendix, Fig. S1A). The fact that none of the control mice but ~70% of the *ITSN* dKO mice fell off the maze during the test period might either be a consequence of reduced anxiety or reflect increased impulsivity, a secondary symptom of ASD (18). While poor motor coordination is not a core symptom of ASD, it is frequently observed in ASD and fragile X syndrome patients (19). *ITSN* dKO mice also exhibited a poor performance when challenged by the beam walking assay (SI Appendix, Fig. S1B). Finally, we found that *ITSN* dKO mice suffer from an altered sleeping pattern (SI Appendix, Fig. S1C), a known comorbidity of ASD in humans (20).

To further explore the causal link between ASD/OCD and intersectin function, we tested whether administration of fluoxetine, a selective inhibitor of serotonin reuptake and first-line OCD treatment (21), can alleviate obsessive jumping in dKO mice. Indeed, chronic administration of fluoxetine over 3 wk significantly decreased the number of observed jumps, and this effect was reversed once the application of fluoxetine was stopped (Fig. 1M). Thus, intersectin dKO mice are a valid model for studying the molecular foundation of repetitive motor routines that are exhibited by a range of ASD and OCD patients with often devastating effects on their ability to cope with life. By recapitulating symptoms of carriers of *de novo* *ITSN1* mutations (7), our mouse model supports the view that these mutations are causative for the neurodevelopmental disorders of the affected patients. We hence used this model to decipher the pathomechanism(s) underlying the behavioral defects.

Structural Alterations of Basal Ganglia upon Loss of *ITSN1/2*. Neuropsychiatric disorders causing repetitive behaviors have been linked to alterations in the basal ganglia, subcortical brain nuclei involved in the formation and execution of motor skills and habits (22, 23). As the entry gate to this circuitry, the striatum receives inputs from cortical areas that are further processed within the basal ganglia and, finally, relayed back to the cortex via the thalamus. Striatal dysfunction in particular has been associated with stereotypic behavior and hyperactivity (24), and alterations in striatal volume have been reported for ASD patients (3, 25). We used magnetic resonance imaging (MRI) (Fig. 2A) paired with volumetric analysis to perform an unbiased brain-wide comparison of brain regions in control and dKO brains. MRI revealed an 11.7% smaller total brain volume of dKO mice (Fig. 2A and B). To assess if the volume reduction of dKO brains affects all brain regions equally, subregions were quantified with respect to their absolute (Fig. 2C and SI Appendix, Table S1) and relative volumes (the fraction of a brain region relative to the total brain; Fig. 2C and SI Appendix, Table S2). Ranking the regional volume changes of dKO vs. 2KO brains by magnitude revealed a strikingly nonuniform volume loss. The most severe volume decrease was observed for the striatum (Fig. 2A and C). This was closely followed by size reductions of the thalamus and pallidum, additional essential information processing centers within the basal ganglia circuitry. Interestingly, some regions like the isocortex or the hippocampus exhibited volume reductions that were smaller than the average brain volume loss. Other brain structures such as the medulla exhibited a volume reduction comparable to the volume loss of the total brain leading to no net change of relative volume (Fig. 2C). In summary, the volume loss of the basal ganglia and particularly the striatum dominates the total

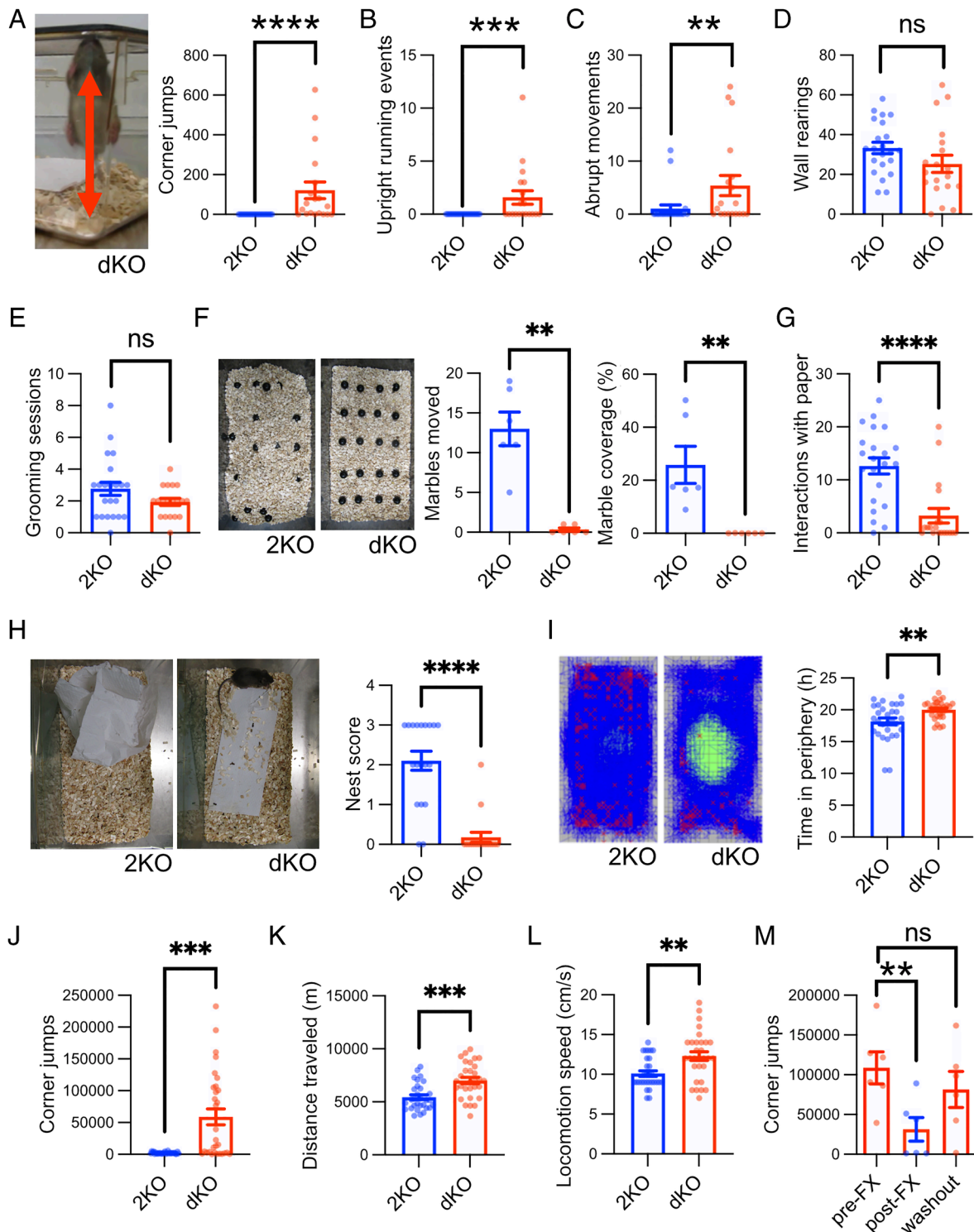


Fig. 1. Loss of intersectins leads to hyperactivity and obsessive stereotypic behavior. (A–E) Intersectin dKO mice display behavioral abnormalities including repetitive jumping behavior. Mice were observed in their home cage environment for 10 min, and the number of corner jumps (A), episodes of upright running (B), abrupt movements (C), rearings at the wall (D), and grooming episodes (E) were scored [N(2KO) = 22 mice, N(dKO) = 19 mice; Mann–Whitney test or unpaired two-tailed *t* test; ***P* < 0.01, ****P* < 0.001, *****P* < 0.0001, ns: not significant]. (F) Intersectin dKO mice fail to bury marbles. Mice were placed in a cage with marbles for 30 min. Afterward, the percentage of marble area covered with bedding material and the number of marbles moved were quantified (N = 6 mice per genotype; Mann–Whitney test; ***P* < 0.01). (G and H) Intersectin dKO mice fail to build nests. Mice were either supplied with a fresh paper towel and observed for 10 min (G) or left in the cage for 24 h (H). For (G) episodes of occupation with paper were scored and for (H) the quality of nest building was graded with 4 being the top score [G: N(2KO) = 22 mice, N(dKO) = 19 mice; unpaired two-tailed *t* test; *****P* < 0.0001; H: N(2KO) = 19 mice, N(dKO) = 17 mice; Mann–Whitney test; *****P* < 0.0001]. (I–L) Infrared-beam-based tracking confirms obsessive behavior of dKO mice and reveals hyperactivity. Mice were tracked in xyz for 24 h via infrared beams (see representative images with tracks in blue and positions of rearing/jumping in red). The time spent in the periphery of the cage (I), the number of z beam breaks in cage corners indicative of high rearing or jumping (J), the distance traveled (K), and the locomotion speed (L) were quantified (N = 30 mice per genotype; Mann–Whitney test or unpaired two-tailed *t* test; ***P* < 0.01, *****P* < 0.001). (M) The OCD medication fluoxetine rescues obsessive behavior of dKO mice. dKO mice with obsessive jumping behavior were treated with fluoxetine for 3 wk, and the number of corner jumps was recorded for 24 h via infrared beams prior to the treatment, immediately after the treatment, and 5 to 6 wk after the treatment (washout). (N = 6 mice; Friedman test with Dunn's multiple comparison test; ***P* < 0.01, ns: not significant).

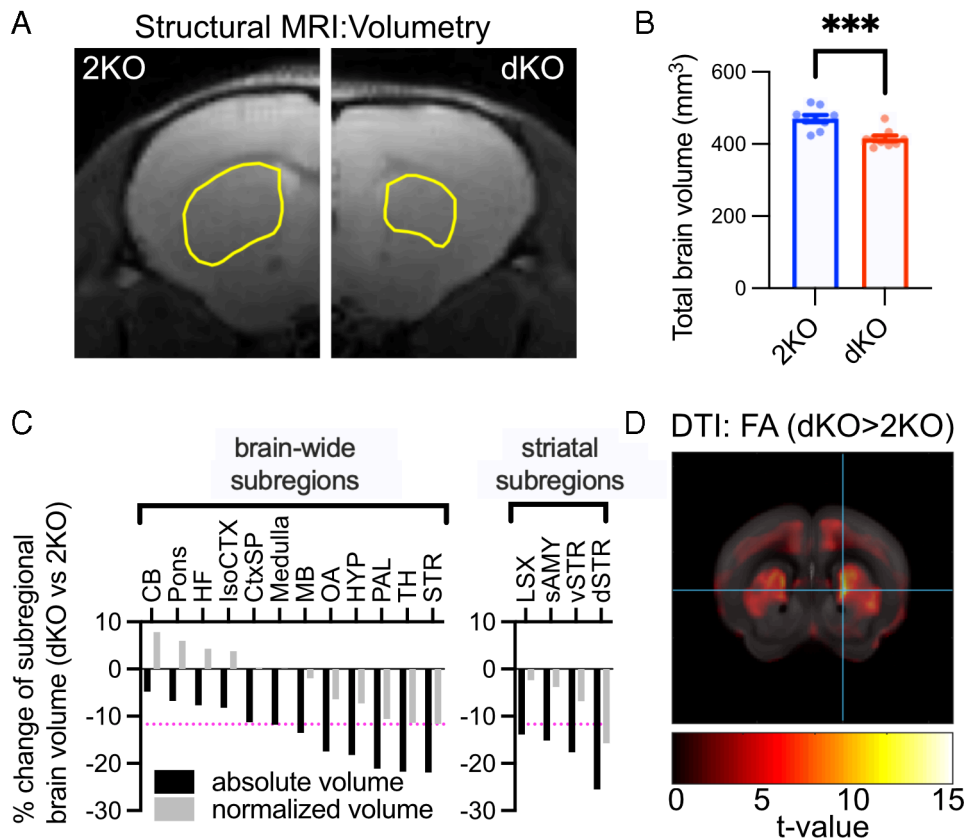


Fig. 2. Morphological alterations of basal ganglia upon loss of ITSN1/2. (A and B) Intersectin dKO mice have smaller brains. Total brain volumes measured by MRI were compared between dKO mice and 2KO mice (A) Representative coronal optical section of one hemisphere per genotype with outlined dorsal striatum (yellow line). (B) Quantification of brain volume (N = 9 mice per genotype; unpaired two-tailed *t* test, ****P* < 0.001). (C) dKO mice have smaller striata. Absolute (black) and normalized regional volume (gray; fraction of total brain volume) of the major brain areas (Left) and striatal subregions (Right) were compared between genotypes and expressed as percent change (dKO vs. 2KO). Detailed values are listed in *SI Appendix, Tables S1 and S2*. Brain structures are ordered by the degree of volume reduction. The magenta dotted line indicates the percent change of total average brain volume. CB, cerebellum; CtxSP, cortical subplate; dSTR, dorsal striatum/caudate putamen; HF, hippocampal formation; HYP, hypothalamus; isoCTX, isocortex; MB, midbrain; LSX, lateral septal complex; OA, olfactory areas; PAL, pallidum; sAMY, striatum-like amygdalar nuclei; STR, striatum; TH, thalamus; vSTR, ventral striatum. (D) dKO mice show microstructural changes in the striatum as measured by DTI. Depiction of color-coded *t*-values of fractional anisotropy (FA) changes in dKO vs. 2KO mice. The detailed voxel-based statistics of FA and axial diffusivity (AD) can be found in *SI Appendix, Fig. S2 and Tables S3 and S4*.

brain size reduction after deletion of ITSN1/2, leading to the underrepresentation of these structures in dKO brains. We find that the striatal volume loss in dKO brains is mainly driven by a reduced size of the caudate putamen (Fig. 2C) (also called dorsal motor striatum), a brain area linked to sensory-motor gating and movement regulation (22, 23).

We used voxel-wise diffusion tensor imaging (DTI), a technique that monitors water diffusion as readout for brain microstructure, to explore potential structural abnormalities within the caudate putamen. Indeed, the DTI analysis revealed increases in two important parameters, axial diffusivity (AD) and fractional anisotropy, in the caudate putamen of dKO mice, indicative of compromised microstructural integrity and a potential decrease in neuronal complexity within this brain region as a consequence of loss of ITSN1/2 (Fig. 2D and *SI Appendix, Fig. S2 and Table S3*).

In summary, dKO brains are characterized by volume loss and microstructural alterations predominantly affecting brain regions involved in movement control. These data are consistent with the abnormal repetitive movement behavior exhibited by dKO mice.

Abnormal Morphology of Striatal Medium Spiny Neurons and Impaired Cortico-Striatal Synaptic Transmission in the dKO Striatum. Since MRI revealed a striking striatal volume reduction in dKO brains, we analyzed the morphology of striatal neurons at high resolution. Approximately 95% of the striatum consists of GABAergic medium spiny neurons (26, 27). To assess

whether the volume reduction was associated with morphological alterations in these neurons, we filled them with biocytin and subsequently stained filled neurons with Alexa Fluor 594-conjugated streptavidin to visualize neuronal arborization and spine density (Fig. 3A–E). Sholl analyses revealed a significantly lower complexity of the dendritic trees of medium spiny neurons from dKO mice (Fig. 3A–C). In addition, we found a significantly reduced density of dendritic spines (Fig. 3D and E) that can serve as a surrogate measure for synaptic contacts (28). These data show that loss of ITSN1/2 critically disturbs the morphological integrity of the major class of striatal output neurons. The decreased morphological complexity of these neurons likely constitutes the cellular correlate of the striatal volume reduction observed in MRI and can explain the increase in AD in DTI and the functional defects underlying stereotypic behavior.

Given the identification of the dorsal striatum as the main morphologically affected brain structure in dKO mice and the link of striatal dysfunction to repetitive movement behavior, we investigated whether cortico-striatal neurotransmission was disturbed in dKO mice. To this aim, we first analyzed basal cortico-striatal neurotransmission using extracellular field recordings in acute coronal brain slices. Cortical afferents were stimulated at the border of the corpus callosum and the dorsolateral striatum (Fig. 3F). Fiber volley amplitudes were unaltered in slices from dKO mice, suggesting a similar recruitment of afferent fibers during stimulation (*SI Appendix, Fig. S3*). In contrast, population spikes caused by the synchronous

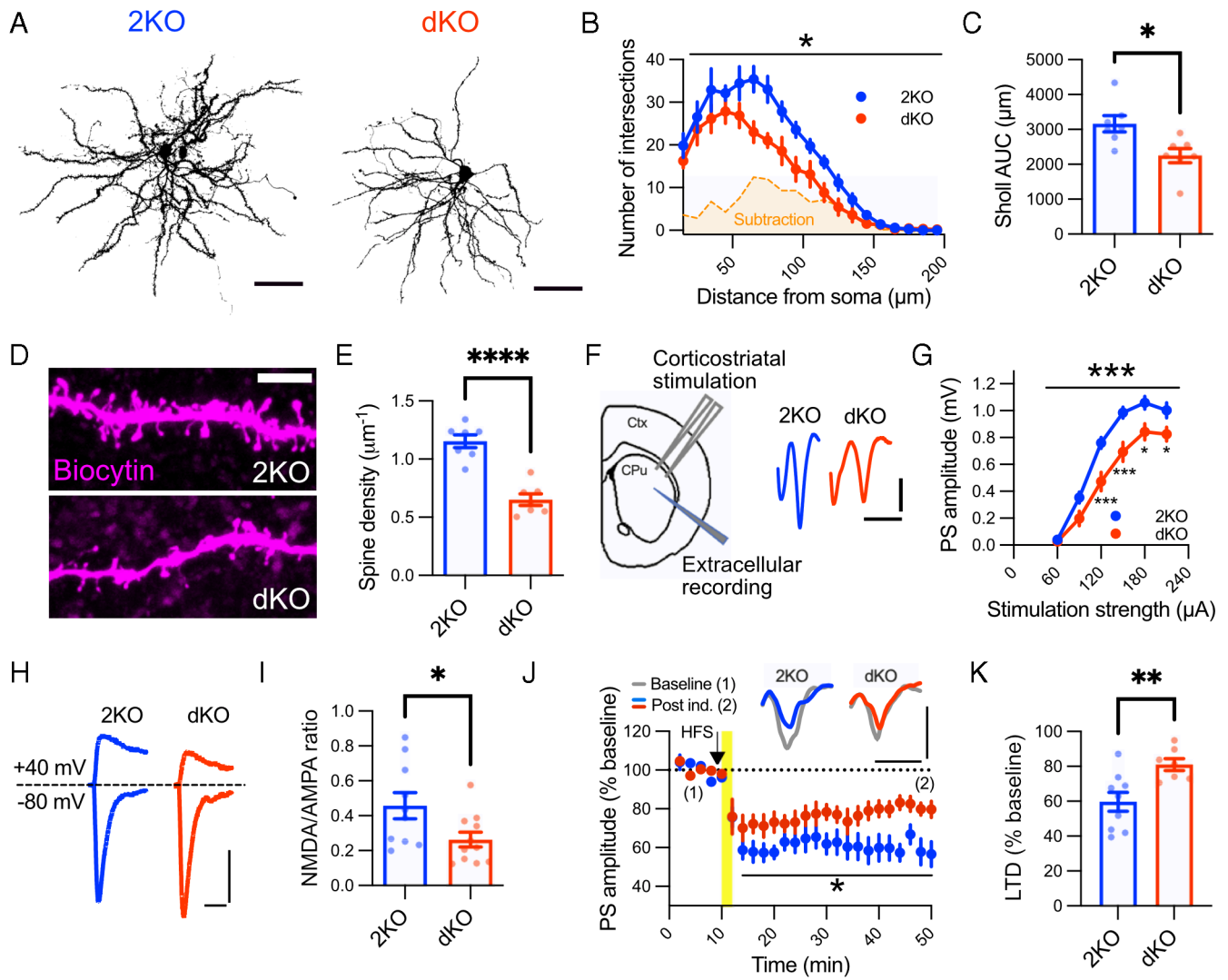


Fig. 3. Impaired neuronal morphology and synaptic function in intersectin dKO mice. (A–C) Intersectin dKO medium spiny neurons are less complex. Maximum intensity projections of biocytin-filled medium spiny neurons from dKO and 2KO mice were thresholded and used to create binary masks for Sholl analysis (A). (B) Two-dimensional Sholl analysis of biocytin-filled neurons. dKO neurons have significantly fewer branches, as visualized by the subtracted area (2KO–dKO, orange shading). Data are shown as the mean number of intersections at 10 μm radial steps from the soma, starting from 15 μm and ending at 195 μm ($N = 7$ cells from at least 3 animals per genotype, two-way RM ANOVA, genotype effect: $*P < 0.05$). (C) The number of dendritic intersections from B was integrated over the complete radial distance under analysis to compare total dendritic intersections between genotypes ($N = 7$ cells from at least 3 animals per genotype, unpaired two-tailed t test $*P < 0.05$). (D and E) dKO medium spiny neurons exhibit a decreased spine density. (D) Maximum intensity projections of dendritic segments filled with biocytin. Note how dKO dendritic segments possess fewer spines on their dendritic branches. (E) Quantification of spine density ($N = 7$ cells from at least 3 animals per genotype, unpaired two-tailed t test $****P < 0.0001$). (F and G) Disturbed basal cortico-striatal transmission in dKO mice. (F) Scheme of electrode placement and representative population spikes evoked with 180 μA stimulation strength in dorsolateral striatum. (G) Population spike amplitudes are significantly smaller in the dKO striatum (2KO: 22 slices from 5 animals, dKO: 21 slices from 5 animals; two-way RM-ANOVA, genotype effect: $***P < 0.001$; followed by Holm–Sidak multiple comparison test, $*P < 0.05$, $***P < 0.001$). (H and I) Decreased NMDA/AMPA current ratios in intersectin dKO medium spiny neurons. (H) Representative traces of NMDAR- and AMPAR-mediated currents measured by whole-cell voltage clamp. (I) Quantification of NMDA/AMPA current ratios (2KO: 10 cells from 4 animals, dKO: 11 cells from 4 animals; unpaired two-tailed t test, $*P < 0.05$). (J and K) Impaired long-term depression in dKO medium spiny neurons. (J, Top) Average population spikes during first 10 min baseline transmission (gray) and during the last 10 min of the experiment (colored). (Bottom) Quantification of population spike amplitude as % of initial 10 min baseline. The arrow and yellow line indicate onset and duration of high-frequency stimulation, respectively (2KO: 9 slices from 3 animals, dKO: 7 slices from 3 animals; two-way RM-ANOVA, genotype effect: $*P < 0.05$). (K) The efficiency of long-term depression was compared by quantification of values of the last 10 min from J (2KO: 9 slices from 3 animals, dKO: 7 slices from 3 animals; unpaired two-tailed t test, $**P < 0.01$).

discharging of targeted medium spiny neurons were significantly reduced in dKO striata (Fig. 3G), indicative of impaired basal synaptic transmission at cortico-striatal synapses. Our analysis of spontaneous excitatory postsynaptic currents (sEPSCs) revealed an increase in the frequency of spontaneous synaptic events (SI Appendix, Fig. S4 A–C), while sEPSC amplitudes were unaltered (SI Appendix, Fig. S4 D and E). These data imply that impaired basal synaptic transmission at cortico-striatal synapses most likely is a consequence of reduced postsynaptic function (e.g., due to reduced spine density and/or altered NMDA receptor currents, see below) rather than defective presynaptic neurotransmission.

Our results suggest that disturbed information flow along the cortico-striatal axis underlies the stereotypic movement behavior of ITSN1/2 dKO animals.

Impaired Striatal Long-Term Plasticity and Reduced NMDA Receptor Function in dKO Mice. Functional alterations within the cortico-striatal circuitry are intimately linked to hyperactivity and stereotypic behaviors in neuropsychiatric disorders such as OCD and ASD (29, 30). In the few known mouse models exhibiting comparable stereotypic jumping, electrophysiological alterations were suggested to be caused by postsynaptic defects at synapses

between cortical afferents and medium spiny neurons due to impaired NMDA receptor signaling (10, 13). To test whether NMDA receptor dysfunction might contribute to intersectin dKO phenotypes in mice, we performed patch-clamp recordings on medium spiny neurons in acute cortico-striatal slices. Indeed, the NMDA to α -amino-3-hydroxy-5-methyl-4-isoxazolepropionic acid (AMPA) receptor current ratios were significantly decreased in dKO brains (Fig. 3 *H* and *I*).

In addition to changes in NMDA receptor function, some mouse models with repetitive behavior phenotypes exhibit alterations in long-term depression (31), the major form of long-term plasticity at cortico-striatal synapses with a critical role for learning motor skills and habit formation (32, 33). Hence, we analyzed long-term plasticity of population spikes in dKO mice. Induction of striatal long-term depression elicited a robust long-term depression response in acute slices from control mice. However, this response was significantly impaired in slices from dKO mice (Fig. 3 *J* and *K*).

To better understand the role of intersectin in the control of NMDA receptor function, we analyzed intersectin's nanoscale localization. Trypsin cleavage assays of isolated mouse brain synaptosomes showed ITSN1 to partition equally between pre- and postsynaptic sites (Fig. 4*A*), consistent with earlier data (34–36). The partial localization of intersectin to postsynaptic sites was confirmed by super-resolution stimulated emission depletion (STED) microscopy of primary neurons in culture (Fig. 4*B*) and by subcellular fractionation experiments, which revealed ITSN1 to be present at the postsynaptic density (PSD) marked by PSD-95, homer1 and the NMDA receptor subunit NR2A (Fig. 4*C*). Furthermore, we found postsynaptic NMDA receptors (i.e., NR2A), PSD-95 and actin to coimmunoprecipitate with endogenous ITSN1 in lysates from mouse brain synaptosomes (Fig. 4*D*). The NMDA receptor subunits NR1 and NR2A were also present in complexes affinity-purified from mouse brain using recombinant GST-tagged ITSN1 SH3 domains as bait (Fig. 4*E*). These results show that intersectin is present at postsynapses where it associates with NMDA receptors and the actin-associated NMDA receptor scaffold protein PSD-95, but not AMPA receptors.

Based on these data we hypothesized that intersectin may act as a scaffold protein that stabilizes NMDA receptors at the PSD. To test this, we isolated synaptic membrane-associated proteins from dKO and control forebrains by biochemical fractionation and compared the levels of NMDA receptors and associated postsynaptic proteins. This analysis revealed a significant decrease in the levels of NR2A/B NMDA receptors, PSD95 and actin, whereas the levels of GluA1/A2-type AMPA receptors were unaltered (Fig. 4 *F* and *G*).

These collective data suggest that intersectin controls the postsynaptic levels of NMDA receptors and, thereby, NMDA receptor function as well as long-term plasticity and movement behavior.

Discussion

In this study, we combined behavioral analyses, structural MRI and DTI, electrophysiology, and biochemistry to identify an important role of intersectins in the structural integrity of basal ganglia, cortico-striatal neurotransmission, and the regulation of movement. Our findings show that intersectins are instrumental for preserving postsynaptic function within the cortico-striatal circuitry and suppress the generation of abnormal repetitive motor routines, which are core symptoms of neuropsychiatric disorders such as ASD and OCD (5). Our results support recent reports associating ITSN1 mutations with neuropsychiatric disorders (7) and provide further evidence for a causal relationship between

defects in intersectin function and neuropsychiatric symptoms including stereotypy.

Disturbances in cortico-striatal transmission and plasticity are strongly implicated in ASD and OCD (4, 37), although it has remained a challenge to pinpoint the underlying pathomechanisms. Among the factors implicated in the development of repetitive behaviors and ASD/OCD are actin-associated postsynaptic scaffold proteins such as Shank2/3 (13, 16, 38, 39), Sapap3 (17), Plenty of SH3s (POSH) (40), and neuroligin1 (9). These proteins are thought to organize NMDA receptor complexes within the PSD (9, 40), likely in part by controlling local actin dynamics. Actin is known to play important roles as a structural component of the PSD and of dendritic spines. The long splice isoform of intersectins that is mostly expressed in the brain harbors a guanine nucleotide exchange factor domain that regulates Cdc42 (41), thereby affecting actin dynamics. In line with this, we observed reduced synaptic actin levels in dKO mice and a prominent reduction in dendritic spine density in striatal neurons from intersectin dKO mice, in agreement with earlier data from cultured neurons (41). Based on these results and the structural resemblance between intersectins and other actin-associated postsynaptic scaffolds (e.g., POSH) as well as their association with NMDA receptors [(42) and this study], we suggest a model according to which intersectins stabilize postsynaptic NMDA receptors by promoting actin polymerization and spine stability (*SI Appendix, Fig. S5A*). Thus, our study on intersectins further enlarges the spectrum of NMDA receptor scaffolding proteins whose loss in mice causes repetitive behaviors (*SI Appendix, Fig. S5B*) and contributes to the notion that defective NMDA receptor function causally underlies ASD/OCD-like behaviors in mouse models and, by extension, in human patients.

We have demonstrated in the past that intersectins fulfill a range of presynaptic functions in hippocampal neurons and at the calyx of Held such as regulating the replenishment of synaptic vesicles (8) and clearing release sites (36, 43). Surprisingly, our analysis at cortico-striatal synapses revealed an increase in the frequency of neurotransmitter release in dKO mice, whereas the amplitude of events (i.e., quantal size) was unchanged (*SI Appendix, Fig. S4*). Although at present we cannot exclude that this alteration in presynaptic function contributes to the observed behavioral phenotype, our electrophysiological data in our view render this possibility unlikely. Moreover, a potential function for intersectins in inhibitory transmission (e.g., in GABAergic medium spiny neurons) will need to be addressed in future studies.

In addition to its effect on NMDA receptor levels, loss of intersectins causes alterations in brain regions known to be involved in movement control such as the striatum and the caudate putamen. A reduction in caudate volume has also been reported in other mouse models displaying repetitive behaviors such as JAKMIP1 KO mice (10) and SLITRK5 KO mice (44). Of note, some ASD mouse models exhibit an enlarged striatum (16), in line with observations in human ASD patients (3, 25). These data suggest that decreases and increases in striatal size can be associated with similar behavioral abnormalities. The fact that increases as well as decreases in the volume of the striatum can be associated with ASD and/or repetitive behaviors supports the notion that the striatum as the input structure for the basal ganglia fulfills a crucial function in the processing of motor information. The striatum via direct and indirect pathways connects to different basal ganglia regions. Activation of medium spiny neurons within the direct pathway promotes motor behavior, while activation of medium spiny neurons in the indirect pathway decreases motor activity (4). Since imbalances between the direct and indirect pathways are assumed to cause repetitive behaviors (45), increased or decreased striatal volume might conceivably cause stereotypy

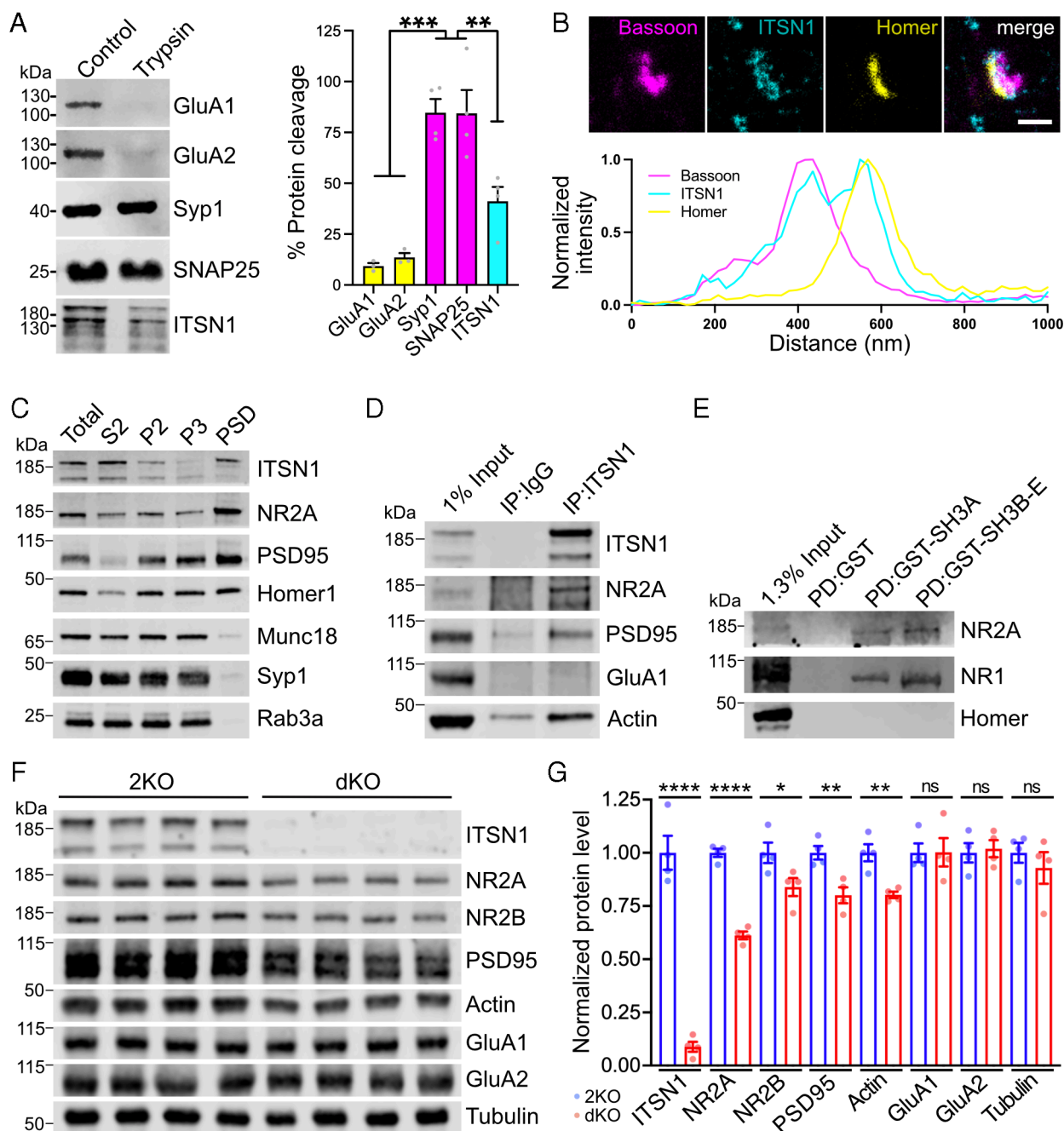


Fig. 4. Intersectin localizes to the postsynapse and stabilizes NMDA receptors. (A) Tryptic digest of synaptosomes reveals postsynaptic localization of ITSN1. Synaptosomes were left untreated or incubated with trypsin and analyzed by immunoblotting. For quantification, trypsin-treated samples were normalized to untreated controls (N = 3 to 4 independent experiments; one-way ANOVA with Tukey post hoc test; ****P < 0.001, ***P < 0.01). (B) Three-channel time-gated STED confirms postsynaptic localization of ITSN1. (Top) Representative image of wild-type neurons immunolabeled with antibodies against the presynaptic marker bassoon, the postsynaptic marker homer, and ITSN1 (scale bar: 500 nm). The white line indicates the position of the normalized fluorescent intensity depicted below. (C) ITSN1 is part of the PSD. Wild-type mouse brain homogenates were subjected to subcellular fractionation, and equal protein amounts of total homogenate (T), cytosolic fraction (S2), synaptosomes (P2), synaptosomal membranes (P3), and PSD were compared by immunoblotting with the indicated markers. (D) ITSN1 forms complexes with NMDA receptors, PSD95 and actin. Coimmunoprecipitation of ITSN1/NMDAR/PSD95/actin complexes from synaptosomal membranes using ITSN1-specific antibodies. Analysis by immunoblotting with the indicated antibodies. (E) Intersectin SH3 domains bind NMDA receptors. GST-intersectin-SH3 domains or GST were incubated with synaptosomal lysate. Analysis by immunoblotting with the indicated antibodies. (F and G) Reduced levels of NMDA receptor subunits in dKO synapses. (F) Immunoblotting for postsynaptic proteins using synaptosomal membrane fractions. Tubulin was used as loading control. (G) Quantification of protein levels normalized to tubulin. For each protein, expression levels from dKO lysates are normalized to 2KO control (N = 4 mice per genotype; unpaired two-tailed t test; *P < 0.05, **P < 0.01, ****P < 0.0001, ns: not significant).

if distinct medium spiny neuron populations are differentially affected.

Previously, ITSN1 has been shown to be expressed at increased levels in Down syndrome (46) being one of the genes located on chromosome 21. Intriguingly, a common mouse model for trisomy 21, Ts65Dn mice, has also been reported to show repetitive

corner jumping (47) suggesting that increased as well as decreased levels of intersectins might be deleterious. In fact, increased levels of intersectin 1 might be harmful since an excess of this scaffold protein might potentially lead to increased NMDA receptor anchorage at the postsynapse and thereby cause aberrant NMDA receptor signaling.

In summary, our findings together with recent genetic data in humans (7, 48, 49) identify intersectins as risk genes for neuropsychiatric diseases. Further investigations on the precise molecular mechanisms that give rise to the changes observed in this study are needed to draw a full picture from gene to behavior and possibly provide an access point for therapeutic interventions.

Materials and Methods

Detailed Materials and Methods are described in *SI Appendix*.

Antibodies. Detailed information on antibodies is provided in *SI Appendix, Table S5*.

Animal Experiments. Animals were group-housed under a 12-h light/dark cycle with food and water ad libitum. All experiments in the present study were conducted in accordance with the guidelines of the LAGeSo Berlin and with their permission. Adult 2KO and dKO mice were observed for 10 min in their home cage environment. For testing nesting, a paper towel was placed into a home cage for 24 h. For assessing marble burying, mice were placed into a cage with 20 marbles for 30 min. To quantitatively assess movement activity, measurements were performed for 24 h using the PhenoMaster ActiMot2 module providing infrared beams in xyz. For testing anxiety-like behavior, mice were observed for 5 min within an elevated plus maze. For testing motor coordination, the ability of mice to walk on a narrow beam was evaluated. Fluoxetine treatment was done with 18 mg/kg per day in the drinking water for 3 wk.

MRI and DTI. MRI was performed on $n = 9$ age-matched 2KO and dKO mice using a 7 Tesla rodent scanner (BioSpec, Bruker, Ettlingen, Germany) equipped with Paravision 6.0.1 software and a ^1H -Cryoprobe. DTI was performed using a spin-echo Stejskal Tanner sequence with geometry matching the anatomical imaging (Two-dimensional spin echo echo-planar imaging (SE-EPI), $5 b = 0$ images, 60 directions with $b = 1,000 \text{ s/mm}^2$, repetition time $TR = 3,500 \text{ ms}$, echo time $TE = 30 \text{ ms}$, matrix size 160×160 , bandwidth = 300 kHz, scan time 15:10 min).

Acute Brain Slice Preparation and Striatal Field and Patch-Clamp Recordings. Acute coronal slices were prepared from 3 to 5 wk (patch clamp) and 9 to 12 wk (field recordings) old 2KO and dKO mice. Mice were killed by cervical dislocation, and brains were rapidly dissected and placed into ice-cold carbogenated (95% O_2 , 5% CO_2) cutting solution (135 mM N-methyl-D-glucamine (NMDG), 1 mM KCl, 1.2 mM KH_2PO_4 , 10 mM glucose, 20 mM choline bicarbonate, 1.5 mM $\text{MgSO}_4 \cdot 7\text{H}_2\text{O}$, 0.5 mM $\text{CaCl}_2 \cdot 2\text{H}_2\text{O}$; pH 7.45; and 305 to 310 mOsm/kg). After removing the cerebellum, brains were glued to the vibratome holder plate. Hemispheres were separated by a medial cut. Subsequently, 300- μm -thick coronal slices containing dorsolateral striatum were prepared in ice-cold carbogenated cutting solution using a vibratome (Leica, VT 1200S).

For extracellular field recordings, a coronal slice was placed in a recording chamber. Responses were evoked after placing the stimulating electrode at the inner edge of the corpus callosum within the dorsolateral striatum. Input-output curves were generated by successively stimulating slices with a biphasic 200 μs current pulse at increasing stimulation intensities and recording the corresponding compound presynaptic action potentials and postsynaptic ensemble somatodendritic depolarizations. High-frequency stimulation-induced long-term depression was triggered by delivering 100 Hz stimulation trains for 1 s (four times, 10 s intertrain interval) at a stimulation intensity that evoked maximum PS amplitude. Depression of striatal responses was recorded by probing PSs every 20 s for an additional 40 min with the same stimulus intensity as used for initial baseline recording. Striatal patch-clamp recordings were performed at 30 °C after identifying medium spiny neurons in the dorsolateral striatum. For measuring the ratio of NMDAR- to AMPAR-mediated synaptic currents, inhibitory GABA_A receptor-mediated transmission was blocked using 20 μM (-)-Bicuculline methiodide supplemented in the recording artificial cerebrospinal fluid. EPSCs were locally evoked using a stimulating electrode placed at the inner edge of the corpus callosum within the dorsolateral striatum, while holding the cell at potentials of -80 mV and $+40 \text{ mV}$, respectively.

Staining and Morphological Analysis of Medium Spiny Neurons. Medium spiny neurons were filled with neurobiotin during patch-clamp experiments. Fixed streptavidin Alexa Fluor™ 594-stained neurons were imaged using an LSM710 laser-scanning microscope.

Preparation of Neuronal Cell Cultures and Time-Gated STED Imaging of Neurons. Hippocampal neurons were isolated from postnatal day 0 to 3 mouse brains. Hippocampi were dissected, placed into ice-cold HEPES-buffered Hank's balanced salt solution (HBSS) containing 20% fetal bovine serum (FBS), and cut with a scalpel into ca. 1-mm³-sized pieces. The tissue pieces were washed with HBSS containing 20% FBS and then with HBSS and afterward were digested for 15 min in digestion buffer (137 mM NaCl, 5 mM KCl, 7 mM Na_2HPO_4 , 25 mM 4-(2-Hydroxyethyl)piperazine-1-ethanesulfonic acid (HEPES), 1 mg/mL trypsin, and 1,500 units DNase, pH 7.2) at 37 °C, followed by another washing step with HBSS and gentle trituration in dissociation buffer (HBSS containing 12 mM MgSO_4 and 1,500 units DNase, pH 7.2). A total of 50,000 hippocampal neurons were plated as 20 μL drops per poly-L-lysine-coated coverslip within a 12-well plate. On DIV14–16, cultured hippocampal neurons were fixed, blocked, and stained with primary antibodies overnight at 4 °C, followed by appropriate secondary antibodies diluted for 1 h at room temperature. STED imaging with time-gated detection was performed on a Leica SP8 TCS STED microscope equipped with a pulsed white-light excitation laser and one STED laser for depletion at 775 nm.

Preparation of Synaptic P3 Fraction from Mouse Brain. Dissected forebrains were homogenized in 8 mL ice-cold homogenization buffer [4 mM HEPES pH 7.4, 320 mM sucrose, 1 mM PMSF, and 1 \times cComplete EDTA-free protease inhibitor cocktail (Sigma-Aldrich)]. The synaptosomal fraction P2, obtained after a series of centrifugation steps, was subjected to hypotonic lysis. Lysed membranes were centrifuged at 25,000 $\times g$ for 30 min at 4 °C to obtain the lysed synaptosomal membrane fraction P3.

Trypsin Cleavage Assay. For the tryptic cleavage of synaptosomes, different trypsin amounts were added to synaptosomal lysates and incubated for 10 min at 30 °C with gentle agitation, followed by centrifugation at 8,700 $\times g$ for 3 min at 4 °C. The resulting pellets were resuspended in 1 \times Laemmli buffer, boiled at 93 °C for 10 min, and analyzed by immunoblotting.

PSD Isolation. A synaptic P3 fraction (see above) was layered on top of a discontinuous sucrose cushion of 0.8, 1.0, and 1.2 M HEPES-buffered sucrose solution and centrifuged at 150,000 $\times g$ for 2 h. Following centrifugation, the synaptic plasma membrane fraction (SPM) at the interphase of 1.0 and 1.2 M sucrose was collected using an 18-G needle on a 1-mL syringe. Of note, 2.5 volumes of 4 mM HEPES were added to the SPM to adjust the sucrose concentration from 1.2 M to 0.32 M. The SPM was then pelleted by centrifugation at 200,000 $\times g$ for 30 min. The resulting pellet was resuspended in 300 μL of 50 mM HEPES buffer containing 2 mM EDTA and combined with 2.7 mL of 0.54% Triton X-100, 2 mM EDTA in 50 mM HEPES, followed by centrifugation at 32,000 $\times g$ for 20 min to obtain the PSD fraction.

Immunoprecipitation. P2 (synaptosomal fraction) was resuspended in lysis buffer (20 mM HEPES, 100 mM KCl, 1 mM MgCl_2 , 1 mM NaF, and 1% sodium taurodeoxycholate). Protein concentration was measured by the BCA assay. Four milligrams of P2 lysate was incubated with 3 μg of primary antibody or with an equivalent amount of IgG control for 1 h on a rotating wheel prior to the addition of 25 μL Pierce™ Protein A/G Magnetic Beads for an additional 3 h. Following incubation, samples were washed 4 \times with lysis buffer, and proteins were eluted with 2 \times Laemmli sample buffer and analyzed by immunoblotting.

Pull-Down Assays. GST-fusion proteins were expressed in *Escherichia coli* (BL21) at 37 °C for 4 h and coupled to glutathione-sepharose beads according to the manufacturer's instructions. Fifty micrograms of GST or GST-fusion protein was incubated with 3 mg of P2 lysate for 4 h under constant rotation at 4 °C. Samples were washed 3 \times using lysis buffer, boiled with 2 \times Laemmli sample buffer, and analyzed by immunoblotting.

SDS-PAGE and Immunoblotting. Samples were separated by sodium dodecyl sulfate polyacrylamide gel electrophoresis (SDS-PAGE), and proteins were transferred onto nitrocellulose membranes. Subsequently, membranes were incubated with primary antibodies (antibody details and dilutions are provided in *SI Appendix, Table S5*) overnight at 4 °C. Afterward, membranes were washed in tris-buffered saline containing 0.1% Tween-20 (TBST), and secondary IRDye 800CW-conjugated antibodies diluted 1:10,000 in TBST were applied for 1 h at room temperature. After washing the membranes again with TBST, signals were detected with the LI-COR Odyssey Fc Imaging system.

Statistics. The specific tests used and their results are stated in *SI Appendix, Table S6*. The number of animals, slices, or cells is indicated in the figure legends and *SI Appendix, Table S6*. In figures, significant differences are indicated by asterisks following this scheme: * $P < 0.05$, ** $P < 0.01$, *** $P < 0.001$, **** $P < 0.0001$. $P > 0.05$ is not significant and indicated as ns. Plotted data points in bar diagrams represent individual mice, individual slices, independent experiments, etc., as specified by N in *SI Appendix, Table S6*. Bars represent the arithmetic mean; error bars represent SEM (if not indicated otherwise in figure legends).

Data, Materials, and Software Availability. The data that support the findings of this study are available from the corresponding authors upon reasonable request. The combined raw data underlying all experiments is too large for permanent storage in a public repository, but will be made available upon request via download links.

ACKNOWLEDGMENTS. We would like to thank Claudia Schmidt and Delia Löwe for technical assistance. Funded by the Deutsche Forschungsgemeinschaft under Germany's Excellence Strategy (EXC-2049 to V.H.), SFB958 (project A01 to V.H. and T.M.) and GRK2737 *STRESSistance* (project A1 to T.M.) and by the

Forschungsinitiative Rheinland-Pfalz BioComp (to T.M.). Funding to S.M., S.P.K. and P.B.S. was provided by the German Federal Ministry of Education and Research (BMBF) under the ERA-NET NEURON scheme (01EW1811) and the Deutsche Forschungsgemeinschaft (Project BO 4484/2-1 and EXC-2049-390688087 NeuroCure).

Author affiliations: ^aLeibniz-Forschungsinstitut für Molekulare Pharmakologie, 13125 Berlin, Germany; ^bDepartment of Nanophysiology, Faculty of Biology, Rheinland-Pfälzische Technische Universität Kaiserslautern-Landau, 67663 Kaiserslautern, Germany; ^cCharité-Universitätsmedizin Berlin, Charité 3R | Replace, Reduce, Refine, 10117 Berlin, Germany; ^dCharité-Universitätsmedizin Berlin, corporate member of Freie Universität Berlin and Humboldt-Universität zu Berlin, Department of Experimental Neurology and Center for Stroke Research, Charitéplatz 1, 10117 Berlin, Germany; ^eCharité-Universitätsmedizin Berlin, NeuroCure Cluster of Excellence and Charité Core Facility 7T Experimental MRIs, 10117 Berlin, Germany; ^fNeuroCure Cluster of Excellence, Charité-Universitätsmedizin Berlin, 10117 Berlin, Germany; and ^gFreie Universität Berlin, Faculty of Biology, Chemistry and Pharmacy, 14195 Berlin, Germany

Author contributions: D.V., V.H., and T.M. designed research; D.V., J.K.S., A.H., S.P.K., S.M., P.B.-S., and T.M. performed research; D.V., J.K.S., A.H., G.K., S.P.K., S.M., P.B.-S., and T.M. analyzed data; G.K. provided training and advice on electrophysiology; and D.V., V.H., and T.M. wrote the paper.

- M. Karno, J. M. Golding, S. B. Sorenson, M. A. Burnam, The epidemiology of obsessive-compulsive disorder in five US communities. *Arch. Gen. Psychiatry* **45**, 1094–1099 (1988).
- A. R. Torres *et al.*, Obsessive-compulsive disorder: Prevalence, comorbidity, impact, and help-seeking in the British National Psychiatric Morbidity Survey of 2000. *Am. J. Psychiatry* **163**, 1978–1985 (2006).
- A. Estes *et al.*, Basal ganglia morphometry and repetitive behavior in young children with autism spectrum disorder. *Autism Res.* **4**, 212–220 (2011).
- M. V. Fuccillo, Striatal circuits as a common node for autism pathophysiology. *Front. Neurosci.* **10**, 27 (2016).
- M. Langen, S. Durston, M. J. Kas, H. van Engeland, W. G. Staal, The neurobiology of repetitive behavior: And men. *Neurosci. Biobehav. Rev.* **35**, 356–365 (2011).
- M. Langen, M. J. Kas, W. G. Staal, H. van Engeland, S. Durston, The neurobiology of repetitive behavior: Of mice. *Neurosci. Biobehav. Rev.* **35**, 345–355 (2011).
- A. L. Bruel *et al.*, ITSN1: A novel candidate gene involved in autosomal dominant neurodevelopmental disorder spectrum. *Eur. J. Hum. Genet.* **30**, 111–116 (2022).
- F. Gerth *et al.*, Intersectin associates with synapsin and regulates its nanoscale localization and function. *Proc. Natl. Acad. Sci. U.S.A.* **114**, 12057–12062 (2017).
- J. Blundell *et al.*, Neurologin-1 deletion results in impaired spatial memory and increased repetitive behavior. *J. Neurosci.* **30**, 2115–2129 (2010).
- J. M. Berg *et al.*, JAKMIP1, a novel regulator of neuronal translation, modulates synaptic function and autistic-like behaviors in mouse. *Neuron* **88**, 1173–1191 (2015).
- T. M. DeLorey, P. Sahbaie, E. Hashemi, G. E. Homanics, J. D. Clark, Gabrb3 gene deficient mice exhibit impaired social and exploratory behaviors, deficits in non-selective attention and hypoplasia of cerebellar vermal lobules: A potential model of autism spectrum disorder. *Behav. Brain Res.* **187**, 207–220 (2008).
- M. R. Etherton, C. A. Blais, C. M. Powell, T. C. Sudhof, Mouse neurexin-1alpha deletion causes correlated electrophysiological and behavioral changes consistent with cognitive impairments. *Proc. Natl. Acad. Sci. U.S.A.* **106**, 17998–18003 (2009).
- H. Won *et al.*, Autistic-like social behaviour in Shank2-mutant mice improved by restoring NMDA receptor function. *Nature* **486**, 261–265 (2012).
- K. M. Jung *et al.*, Uncoupling of the endocannabinoid signalling complex in a mouse model of fragile X syndrome. *Nat. Commun.* **3**, 1080 (2012).
- G. E. Demas, R. J. Nelson, B. K. Krueger, P. J. Yarowsky, Spatial memory deficits in segmental trisomic Ts65Dn mice. *Behav. Brain Res.* **82**, 85–92 (1996).
- J. Peca *et al.*, Shank3 mutant mice display autistic-like behaviours and striatal dysfunction. *Nature* **472**, 437–442 (2011).
- J. M. Welch *et al.*, Cortico-striatal synaptic defects and OCD-like behaviours in Sapap3-mutant mice. *Nature* **448**, 894–900 (2007).
- A. K. Sauer, J. E. Stanton, S. Hans, A. M. Grabrucker, "Autism spectrum disorders: Etiology and pathology" in *Autism Spectrum Disorders*, A. M. Grabrucker, Ed. (Exon Publications, Brisbane (AU), 2021), 10.36255/exonpublications.autismspectrumdisorders.2021.etiology.
- S. De Rubeis, C. Bagni, Regulation of molecular pathways in the Fragile X Syndrome: Insights into autism spectrum disorders. *J. Neurodev. Disord.* **3**, 257–269 (2011).
- D. Burman *et al.*, Sleep and autism spectrum disorder: A comprehensive review of diagnosis, markers, interventions, and treatments. *Sleep Vigilance* **7**, 9–22 (2023), 10.1007/s41782-022-00222-3.
- N. Maneeton *et al.*, Fluoxetine in acute treatment of children and adolescents with obsessive-compulsive disorder: A systematic review and meta-analysis. *Nord J. Psychiatry* **74**, 461–469 (2020).
- A. M. Graybiel, S. T. Grafton, The striatum: Where skills and habits meet. *Cold Spring Harb. Perspect. Biol.* **7**, a021691 (2015).
- S. Grillner, B. Robertson, M. Stephenson-Jones, The evolutionary origin of the vertebrate basal ganglia and its role in action selection. *J. Physiol.* **591**, 5425–5431 (2013).
- G. Kohls, B. E. Yerys, R. T. Schultz, Striatal development in autism: Repetitive behaviors and the reward circuitry. *Biol. Psychiatry* **76**, 358–359 (2014).
- J. Naaijen *et al.*, Striatal structure and its association with N-Acetylaspartate and glutamate in autism spectrum disorder and obsessive compulsive disorder. *Eur. Neuropsychopharmacol.* **28**, 118–129 (2018).
- C. R. Gerfen, Synaptic organization of the striatum. *J. Electron Microsc. Tech* **10**, 265–281 (1988).
- J. M. Kemp, T. P. Powell, The structure of the caudate nucleus of the cat: Light and electron microscopy. *Philos. Trans. R Soc. Lond B Biol. Sci.* **262**, 383–401 (1971).
- A. D. Bird, H. Cuntz, Dissecting sholl analysis into its functional components. *Cell Rep.* **27**, 3081–3096.e5 (2019).
- D. Palumbo, R. Kurlan, Complex obsessive compulsive and impulsive symptoms in Tourette's syndrome. *Neuropsychiatr. Dis. Treat* **3**, 687–693 (2007).
- J. M. van der Meer *et al.*, Are autism spectrum disorder and attention-deficit/hyperactivity disorder different manifestations of one overarching disorder? Cognitive and symptom evidence from a clinical and population-based sample. *J. Am. Acad. Child. Adolesc. Psychiatry* **51**, 1160–1172.e3 (2012).
- G. Martella *et al.*, The neurobiological bases of autism spectrum disorders: The R451C-neuligin 3 mutation hampers the expression of long-term synaptic depression in the dorsal striatum. *Eur. J. Neurosci.* **47**, 701–708 (2018).
- H. H. Yin *et al.*, Dynamic reorganization of striatal circuits during the acquisition and consolidation of a skill. *Nat. Neurosci.* **12**, 333–341 (2009).
- C. M. Gremel *et al.*, Endocannabinoid modulation of orbitostriatal circuits gates habit formation. *Neuron* **90**, 1312–1324 (2016).
- S. Thomas *et al.*, Intersectin regulates dendritic spine development and somatodendritic endocytosis but not synaptic vesicle recycling in hippocampal neurons. *J. Biol. Chem.* **284**, 12410–12419 (2009).
- A. Pechstein *et al.*, Regulation of synaptic vesicle recycling by complex formation between intersectin 1 and the clathrin adaptor complex AP2. *Proc. Natl. Acad. Sci. U.S.A.* **107**, 4206–4211 (2010).
- M. Japel *et al.*, Intersectin-mediated clearance of SNARE complexes is required for fast neurotransmission. *Cell Rep.* **30**, 409–420.e6 (2020).
- E. Burguiere, P. Monteiro, L. Mallet, G. Feng, A. M. Graybiel, Striatal circuits, habits, and implications for obsessive-compulsive disorder. *Curr. Opin. Neurobiol.* **30**, 59–65 (2015).
- C. M. Durand *et al.*, Mutations in the gene encoding the synaptic scaffolding protein SHANK3 are associated with autism spectrum disorders. *Nat. Genet.* **39**, 25–27 (2007).
- S. Berkel *et al.*, Mutations in the SHANK2 synaptic scaffolding gene in autism spectrum disorder and mental retardation. *Nat. Genet.* **42**, 489–491 (2010).
- M. Yao *et al.*, POSH regulates assembly of the NMDAR/PSD-95/Shank complex and synaptic function. *Cell Rep.* **39**, 110642 (2022).
- N. K. Hussain *et al.*, Endocytic protein intersectin-1 regulates actin assembly via Cdc42 and N-WASP. *Nat. Cell Biol.* **3**, 927–932 (2001).
- T. Nishimura *et al.*, Role of numb in dendritic spine development with a Cdc42 GEF intersectin and EphB2. *Mol. Biol. Cell* **17**, 1273–1285 (2006).
- T. Sakaba *et al.*, Fast neurotransmitter release regulated by the endocytic scaffold intersectin. *Proc. Natl. Acad. Sci. U.S.A.* **110**, 8266–8271 (2013).
- S. V. Shmelkov *et al.*, Slitrk5 deficiency impairs corticostriatal circuitry and leads to obsessive-compulsive-like behaviors in mice. *Nat. Med.* **16**, 598–602 (2010).
- J. T. Ting, G. Feng, Neurobiology of obsessive-compulsive disorder: Insights into neural circuitry dysfunction through mouse genetics. *Curr. Opin. Neurobiol.* **21**, 842–848 (2011).
- M. P. Hunter *et al.*, Intersectin 1 contributes to phenotypes in vivo: Implications for Down's syndrome. *Neuroreport* **22**, 767–772 (2011).
- C. A. Turner *et al.*, Spontaneous stereotypy in an animal model of Down syndrome: Ts65Dn mice. *Behav. Genet.* **31**, 393–400 (2001).
- S. J. Sanders *et al.*, De novo mutations revealed by whole-exome sequencing are strongly associated with autism. *Nature* **485**, 237–241 (2012).
- M. Fromer *et al.*, De novo mutations in schizophrenia implicate synaptic networks. *Nature* **506**, 179–184 (2014).